Swift Nanopattern Formation of PS-*b*-PMMA and PS-*b*-PDMS Block Copolymer Films Using a Microwave Assisted Technique

Dipu Borah,[†,‡,§] Ramsankar Senthamaraikannan,[†,‡] Sozaraj Rasappa,[†,‡] Barbara Kosmala,[†,§] Justin D Holmes,[†,‡,§] and Michael A Morris[†,‡,§,*]

[†]Materials Chemistry Section, Department of Chemistry, University College Cork, College Road, Cork, Ireland, [‡]Centre for Adaptive Nanostructures and Nanodevices (CRANN), Trinity College Dublin, College Green, Dublin 2, Ireland, and [§]Tyndall National Institute, Lee Maltings, Prospect Row, Cork, Ireland

ABSTRACT Microphase separation of block copolymer (BCPs) thin films has high potential as a surface patterning technique. However, the process times (during thermal or solvent anneal) can be inordinately long, and for it to be introduced into manufacturing, there is a need to reduce these times from hours to minutes. We report here BCP self-assembly on two different systems, polystyrene-*b*-polymethylmethacrylate (PS-*b*-PMMA) (lamellar- and cylinder-forming) and polystyrene-*b*-polydimethylsiloxane (PS-*b*-PDMS) (cylinder-forming) by microwave irradiation to achieve ordering in short times. Unlike previous reports of microwave assisted microphase segregation, the microwave annealing method reported here was undertaken without addition of solvents. Factors such as the anneal time and temperature, BCP film thickness, substrate surface type, *etc.* were investigated for their effect of the ordering behavior. The microwave technique was found to be compatible with graphoepitaxy, and in the case of the PS-*b*-PDMS system, long-range translational alignment of the BCP domains was observed within the topographic patterns. To demonstrate the usefulness of the method, the BCP nanopatterns were turned into an 'on-chip' resist by an initial plasma etch and these were used to transfer the pattern into the substrate.

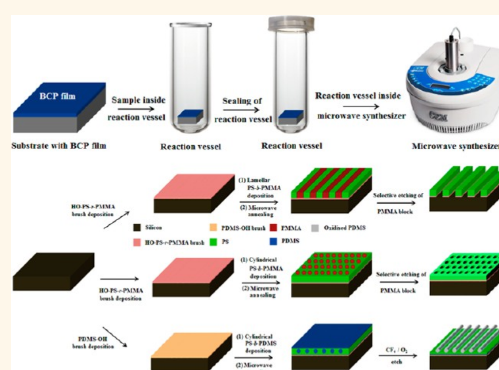

KEYWORDS: polymer brushes · block copolymers · microwave anneal · self-assembly · graphoepitaxy · plasma etching · silicon nanostructures

The semiconductor industry is moving toward ever smaller critical device dimensions;[1] however, conventional lithography based "top-down" process is approaching technical and cost limits.[2−4] The self-assembly of block copolymers (BCPs) might form the basis for a new lithography offering the promise for the fabrication of nanopatterns of sub-20 nm scale features without the need for expensive light sources.[5] BCP nanolithographic methods find industrial applications in the fabrication of nanowires,[6] magnetic storage devices,[7] nanoporous membranes,[8] *etc.* Excellent control over pattern dimension and structure can be achieved in BCP systems through variation of the molecular weight (N), relative volume fraction (ϕ) and the segmental interaction parameter (χ) and a number of different morphological structures *viz.*, lamellar, cylindrical, spherical, gyroid, *etc.*[9,10] can all be formed.

Despite the promise of BCP techniques and very significant research efforts, a number of challenges exist.[11−22] One of these is the processing time to achieve microphase separation as the ordering of BCP domains are generally achieved by thermal or solvent swelling approaches that can be time-consuming.[17,18] Herein is reported a possible alternative to these methodologies that promises very short processing times based around developing a nonconventional microwave assisted BCP microphase separation process. Two different BCP systems, polystyrene-*b*-polymethylmethacrylate (PS-*b*-PMMA) (lamellar- and cylinder-forming) and polystyrene-*b*-polydimethylsiloxane (PS-*b*-PDMS)

* Address correspondence to m.morris@ucc.ie.

Received for review November 20, 2012 and accepted July 16, 2013.

Published online July 16, 2013
10.1021/nn4035519

© 2013 American Chemical Society

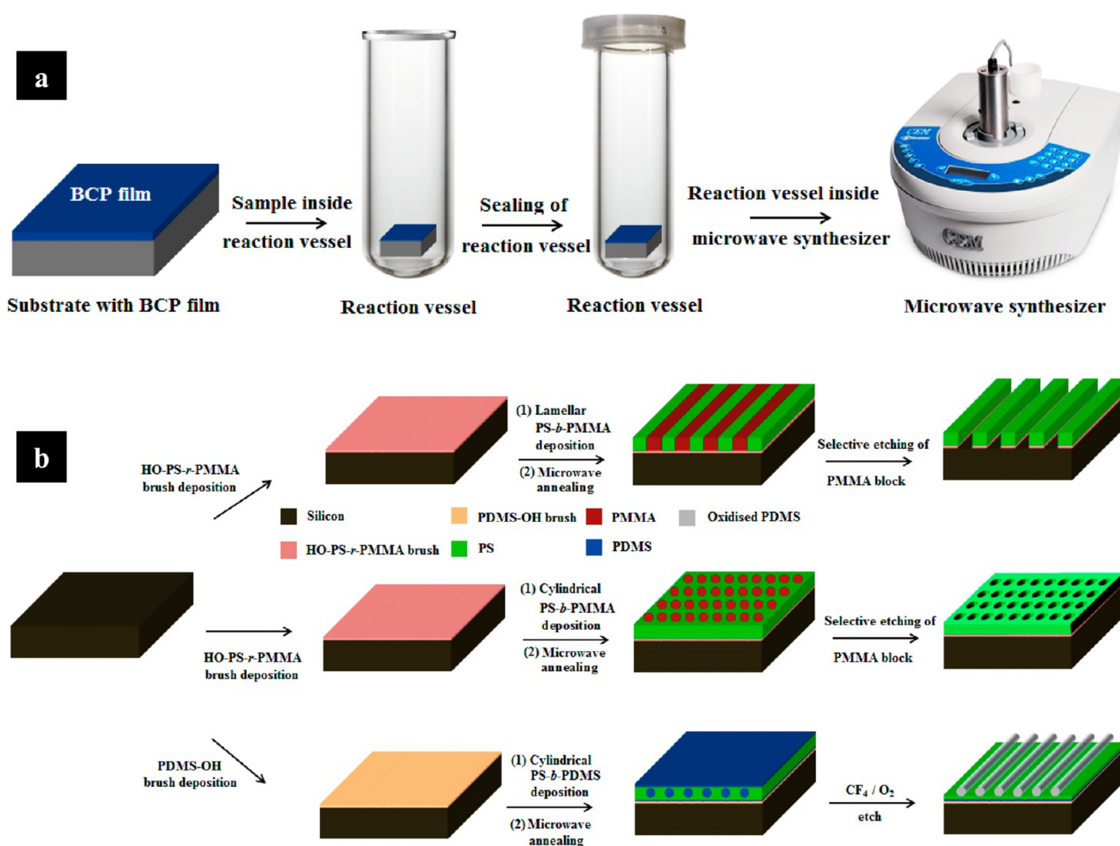

Scheme 1. (a) Scheme depicting the process of microwave annealing of BCP films in the absence of solvent: BCP film onto substrate, putting the sample into the reaction vessel and sealing off, and finally microwave annealing in the synthesizer to achieve BCP ordering. (b) Schematic representation of the process flow showing BCP self-assembly on silicon substrate precoated with hydroxyl-terminated polymer brushes and subsequent plasma etching. See text for details

(cylinder-forming) were considered in the present investigation. These are two of the most heavily investigated systems and microphase separated thin film nanopattern structures are formed by extended vacuum annealing (of the order of 6–48 h[23–30]) and solvent annealing (of the order of 2–24 h[31–41]). It is demonstrated here that microphase segregation of BCPs compatible with that achieved by standard annealing methods can be accomplished by microwave treatment.[42,43] Compared to previous reports on the use of microwave heating,[42,43] no solvent is used and good microphase separation can be achieved at planar and topographically patterned substrates. To demonstrate the effectiveness of the method and the regularity of the pattern with film depth, the patterns were transferred to the substrate.

RESULTS

A schematic depicting the microwave anneal of BCPs is presented in Scheme 1a. It should be noted that all the microwave irradiated experiments were performed without the aid of solvent unlike the work reported by Buriak *et al.*[43] As can be seen in Scheme 1a, the substrate coated with BCP was placed in a reaction tube specially designed for microwave experiments, sealed, and then irradiated with microwave energy. The detailed self-assembly steps starting with hydroxyl-terminated polymer brush grafting, resultant structure formation and plasma etching steps are schematically shown in Scheme 1b. A number of parameters were investigated to demonstrate the diversity of the microwave anneal process which includes: microwave irradiation time and temperature, BCP morphology and molecular weight, substrate resistivity, and directed self-assembly by graphoepitaxy.

Microwave Assisted Self-Assembly of BCPs. The PS-*b*-PMMA BCPs were spin-casted from toluene solutions onto the polymer brush coated substrates prior to irradiation with microwave energy. The thickness of the as-cast BCP films were determined by ellipsometry and the data are compiled in Table 1. It can be seen in Table 1 that the average film thickness is ~40 nm for 1.0 wt % coating solutions irrespective of the PS-*b*-PMMA molecular weight, but this thickness increases with the concentration of the polymer solution as expected. Symmetric PS-*b*-PMMA thin films prepared the brush layer and exhibit a lamellar morphology consisting of vertically orientated lamellae of PS and PMMA.

Figure 1a–c shows the top-down scanning electron microscope (SEM) images of PMMA etched lamellar PS-*b*-PMMA BCP of three different molecular weights

TABLE 1. Water Contact Angle and Film Thickness (Ellipsometry) of Polymer Brush Layers and BCP Films on Substrate Surfaces[a]

material	deposition condition	contact angle/(deg)	thickness/nm	pitch from AFM, SEM/nm
RPB/Si substrate	annealed/cleaned	83.7 ± 1.5	5.1	-
PDM/Si substrate	annealed/cleaned	112.6 ± 1.5	4.3	-
BC36/Si substrate	RPB + BC36 (0.7 wt %)	-	30.3	26
BC36/Si substrate	RPB + BC36 (1.0 wt %)	-	35.4	26
BC36/Si substrate	RPB + BC36 (1.5 wt %)	-	38.7	26
BC74/Si substrate	RPB + BC74 (1.0 wt %)	-	39.2	42
BC104/Si substrate	RPB + BC104 (1.0 wt %)	-	40.6	54
BC67/Si substrate	RPB + BC67 (1.0 wt %)	-	33.1	36
BC67/Si substrate	RPB + BC67 (2.0 wt %)	-	48.7	36
BC67/Si substrate	RPB + BC67 (3.0 wt %)	-	56.3	36
BC45/Si substrate	PDM + BC45 (1.0 wt %)	-	36.6	35

[a] The table includes the pitch period of the BCP calculated from the FFT of AFM topography/SEM images (see Figure S2 in Supporting Information for AFM images).

on silicon substrates precoated with HO-PS-*r*-PMMA brush (ellipsometry thickness ~5.1 nm (see Figure S1 in Supporting Information for TEM cross-section of brush layer)) (note that PMMA removal was used to develop image contrast). The BCP films were microwave irradiated at 323 K for 60 s, and sufficient microwave power (~100 W) was used to maintain this temperature. It is apparent that the process produced ordering of the BCP irrespective of the molecular weight. Interestingly, the optimum pattern ordering is observed with the lowest molecular weight PS-*b*-PMMA, BC36. This can be explained by the lower molecular weight favoring greater molecular motion allowing the minimum energy conformation to be achieved during annealing. The SEM cross-sectional images presented in insets to Figure 1 demonstrate PMMA removal and the formation of PS line structures. The lamellar repeat distances are compiled in Table 1 and it is clear that PS pitch and feature size are directly determined by the molecular weight of the BCP. The dimensions are close to those we have previously measured using thermal anneal processes and suggests that no polymer rearrangements, *etc.* are caused by the microwave technique.

The results for the cylinder-forming PS-*b*-PMMA, BC67 on substrate precoated with HO-PS-*r*-PMMA brush and microwave annealed at 323 K for 60 s is presented in Figure 1d. The BCP film was cast from a 2.0 wt % of the polymer solution in toluene yielding a film thickness of ~49 nm (Table 1). The top-down SEM images of the etched film confirm a vertical alignment of cylinders and suggest removal of the PMMA domains. It was observed that there is minor enlargement of the pore diameter (pores result from PMMA cylinder removal) during the selective etch process. Comparison of SEM and AFM images suggests that the pore size is 16.2 nm compared to a cylinder size of 18.7 nm measured from equivalent AFM images. However, the center-to-center distance between pores was not modified during the PMMA removal process, and the mean value obtained was 35.1 nm in agreement with AFM data (Table 1). The increased pore diameter is probably due to isotropic etching of the polymer and/or possibly plasma induced strong cross-linking of the PS matrix.[44]

Figure 1e shows the results of the oxidized PDMS cylinders after a sequential CF_4 and O_2 etches obtained from the microphase separated PS-*b*-PDMS film on PDMS−OH brush (ellipsometry thickness ~4.3 nm) microwave annealed at 323 K for 60 s. The SEM image shows a single monolayer of PDMS cylinders and clearly demonstrates the efficacy of etch chemistry to reveal the cylindrical patterns. It is evident from the data in Figure 1e that well-ordered phase separation is seen over macroscopic distances. The mean PDMS cylinder spacing, L_0, and line width, $\langle d \rangle$, were found to be 36.4 nm and 16.2 nm, respectively. It can also be seen from the image that the oxidized PDMS domains have become rounded during the etch process indicating that it is partially isotropic. The oxidation of the PDMS cylinders during this pre-etch step is confirmed by FTIR with the detection of a Si−O−Si signal at 1100 cm^{-1}[45] as displayed in Figure 1f. Dewetting is a major issue with high χ BCP systems such as PS-*b*-PDMS leading to multilayer pattern formation in some locations on the substrate upon solvent annealing. However, the dewetting was not there in microwave annealed PS-*b*-PDMS films which is advantageous in getting uniform monolayer of *in-plane* PDMS cylinders for subsequent pattern transfer to underlying silicon substrate. Absence of dewetting could be due to transient irradiation time as compared to a longer solvent anneal time usually followed.

Effect of BCP Film Thickness on Microwave Assisted Self-Assembly. Microphase separation derived BCP thin film nanopatterns can display orientations strongly dependent on film thickness.[46−48] To verify such effects in microwave processed films, a systematic study of the film thickness effect on self-assembly on BC36 and BC67 was performed. Results are presented in Figure 2. The anneal temperature and time were fixed at 323 K and 60 s, respectively. SEM images were taken at different locations on the substrate and show that

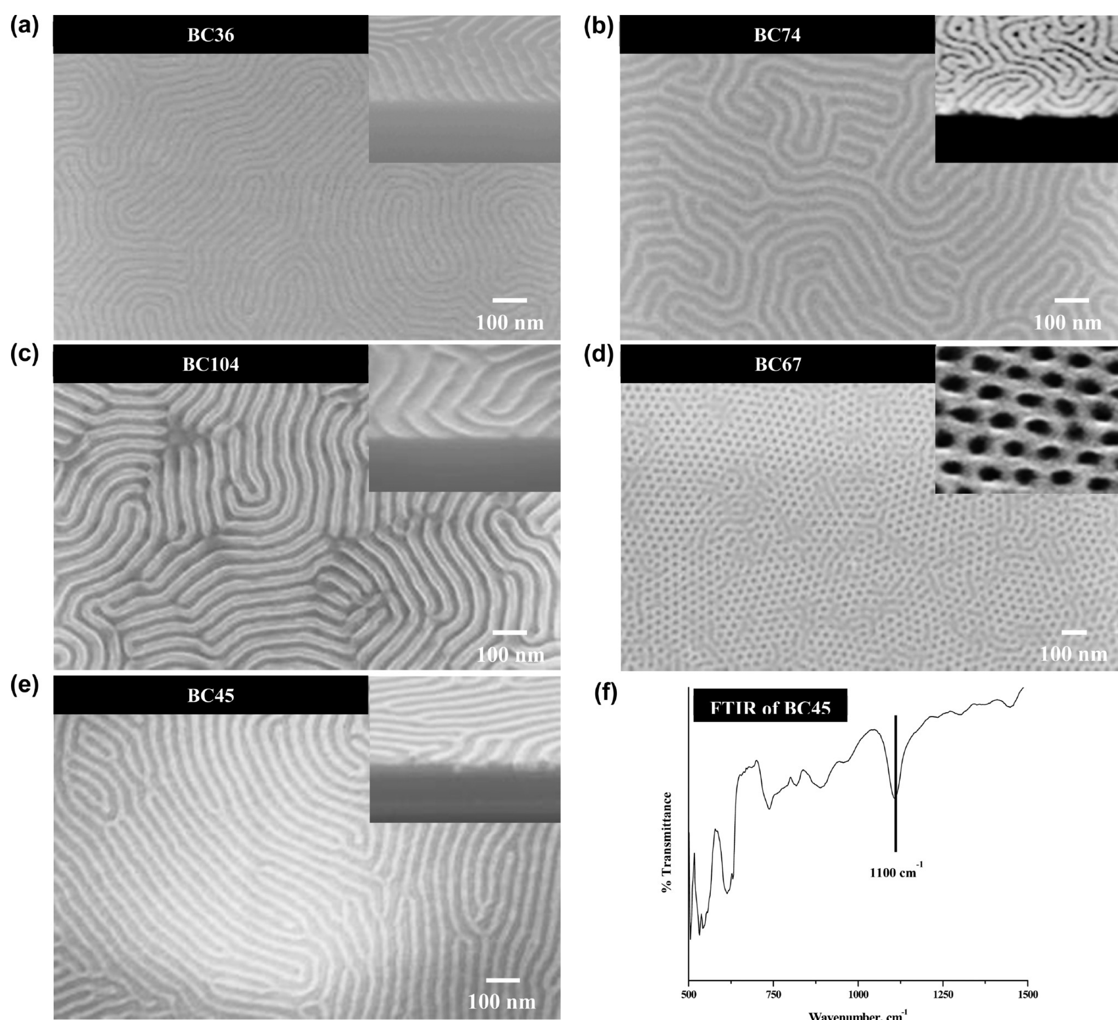

Figure 1. Top-down and off-axis (inset) cross-sectional SEM images of PS-*b*-PMMA and PS-*b*-PDMS BCP films after selective plasma removal of the PMMA component, and the top PDMS wetting layer and partial PS matrix for PS-*b*-PMMA and PS-*b*-PDMS, respectively (light gray lines/matrix are PS/PDMS and darker lines/holes are voids created following PMMA/PS removal) on silicon substrates as labeled in the images. BCP films were microwave annealed at 323 K for 60 s. FTIR spectrum of the oxidized PDMS cylinders formed from the PS-*b*-PDMS (BC45) using CF_4 and O_2 etches.

the orientation is homogeneous over the entire surface. It is evident that 1.0 wt % of BC36 on HO-PS-*r*-PMMA brush gives the best results with a high degree of ordering and uniform film thickness. However, at the other concentrations, the films became rough on microwave irradiation and significant areas that were featureless can be identified in the SEM images. This is consistent with thicknesses that are not commensurate with the domain spacing and parallel alignment or absence of pattern in some areas.

It can be seen that microwave annealing of BC67 on HO-PS-*r*-PMMA brush can result in vertical, parallel or mixed orientation of the PMMA cylinders dependent on film thickness as seen in thermal or solvent annealed processing.[46−49] For a 1.0 wt % BCP casting solution (∼33 nm thickness), vertical and parallel cylinder orientation can be observed as well as featureless regions (Figure 2). We suggest this film thickness is below that need to produce a coherent film thickness with featureless regions representing polymer-free areas and changes in orientation reflecting changing thickness within BCP islands. However, hexagonally ordered cylindrical PMMA microdomains in a PS matrix oriented perpendicular to the substrate are observed with BCP concentrations of 2.0 and 3.0 wt %. This suggests the film thickness allows regular coating and that the brush preferentially favors this orientation. This hexagonal phase BCP exhibits a hexagonal arrangement of phase of PMMA cylinders in a PS matrix with a center-to-center spacing of about 35 nm.

Effect of Microwave Anneal Time on Self-Assembly. Previous studies of conventional thermal annealing shows that BCP morphology and ordering depend upon the anneal time,[13] and therefore, a series of experiments were undertaken here. Films were microwave irradiated for various lengths of time (30−360 s) at a constant temperature of 323 K with sufficient microwave power (∼100 W) to maintain the temperature

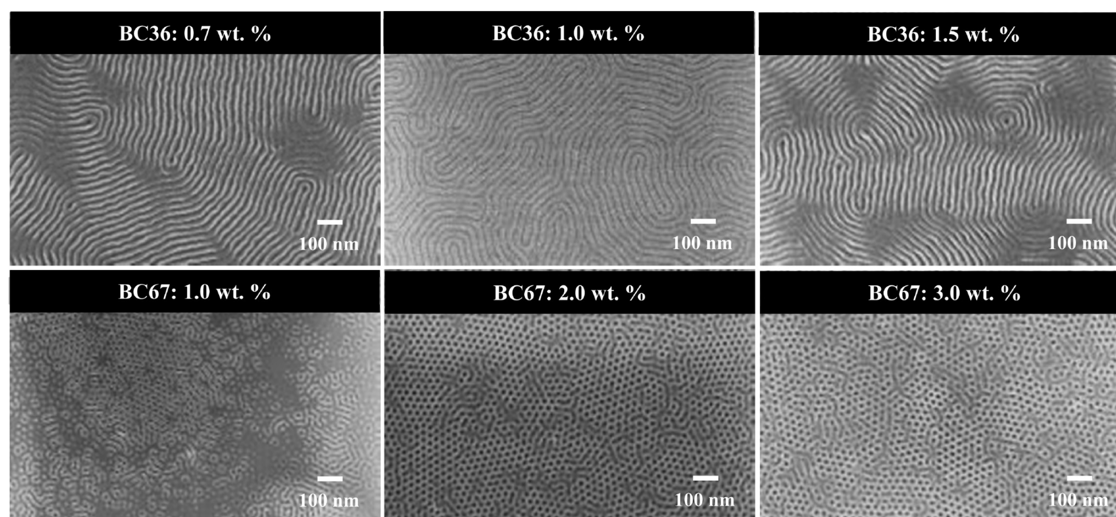

Figure 2. Top-down SEM images of the PS-*b*-PMMA BCP (BC36 and BC67) films after selective plasma removal of the PMMA component (light gray lines are PS and darker lines are voids created following PMMA removal). The BCP film thicknesses were varied as labeled in the images and were microwave annealed at 323 K for 60 s.

and the results are presented in Figure 3. The results for lamellar PS-*b*-PMMA BCPs show microphase separation across the surface irrespective of anneal time and molecular weight. However, the patterns became more disordered and increase in the number of defect sites with the increase of anneal time particularly with lower molecular weight PS-*b*-PMMA (BC36). This might suggest that extended annealing periods cause such extensive molecular motion in the small, more mobile system that the effective order−disorder phase boundary is crossed and disorder is 'frozen-in' on cooling, *etc.*

The results of BC67 system reveal an interesting trend as can be seen in Figure 3. At short and long anneal times, much higher concentrations of pattern orientation and structural defects are observed, wheras a 60 s anneal appears to be optimum for generating patterns of good structural order. As above, it would appear that longer anneal periods lead to structural disorder due to high chain mobility. It might be suggested that a 30 s anneal is not long enough to reach structural order. It would thus appear that the microwave anneal method as used here is somewhat complex and the structures observed are kinetically 'trapped' rather than a progression toward the thermodynamically stable state as seen in conventional methods.

The time dependence of microwave annealing on the microphase separation of PS-*b*-PDMS BCP thin films is presented in Figure 3. As seen for PS-*b*-PMMA, the patterns became more disordered and defects density increases with anneal time. The mean PDMS cylinder spacing, L_0, and line width, $\langle d \rangle$, were found to be 36.2 and 15.9 nm, respectively.

Effect of Microwave Anneal Temperature on Self-Assembly. The process mechanism described above suggests that the temperature used in the microwave assisted assembly process might be important and data are presented in Figure 4. For PS-*b*-PMMA BCPs, the anneal temperature was chosen in the range of 323−453 K (60 s anneal period), below and above the glass transition temperatures (Tg) of PS and PMMA blocks. Generally, the anneal temperature has a lesser effect than might be first considered. From Figure 4, it is evident for all the systems studied that BCP film ordering deteriorates as the temperature is increased (most notably for lower molecular weight BCPs) and that optimum structural order is attained well below Tg. The lack of very dramatic effects suggests that thermal motion of the polymer chains is not very important and ordering arises from chain motions caused by microwave excitement and that the 'effective' temperature of the film is significantly higher than the process temperature as measured in the instrument.

Figure 4 shows the temperature evolution of PS-*b*-PDMS BCP ordering in the temperature range of 323−453 K. A shorter anneal time of 30 s was considered optimum based on the results of time evolution described above. Figure 4 reveals a similar temperature dependence as that seen for the PS-*b*-PMMA system with less structurally well-defined patterns observed at higher temperatures. Also observed was a small increase in the mean PDMS and at the highest temperature the cylinder spacing and line width were found to be 38.3 and 17.7 nm, respectively, compared to corresponding values of 36.2 and 15.9 nm seen at the lowest temperature. This is consistent with some 'freezing-in' of free volume caused by microwave excited motion of both blocks.

Effect of Substrate Surface Type on Microwave Assisted Self-Assembly. A wide range of substrates *e.g.*, silicon, silicon dioxide, silicon-on-insulator, silicon nitride, *etc.*, were investigated here and some dependence was observed. Note that the resistivity of the substrates used varied in the following way: bulk Si, SiO_2/bulk Si,

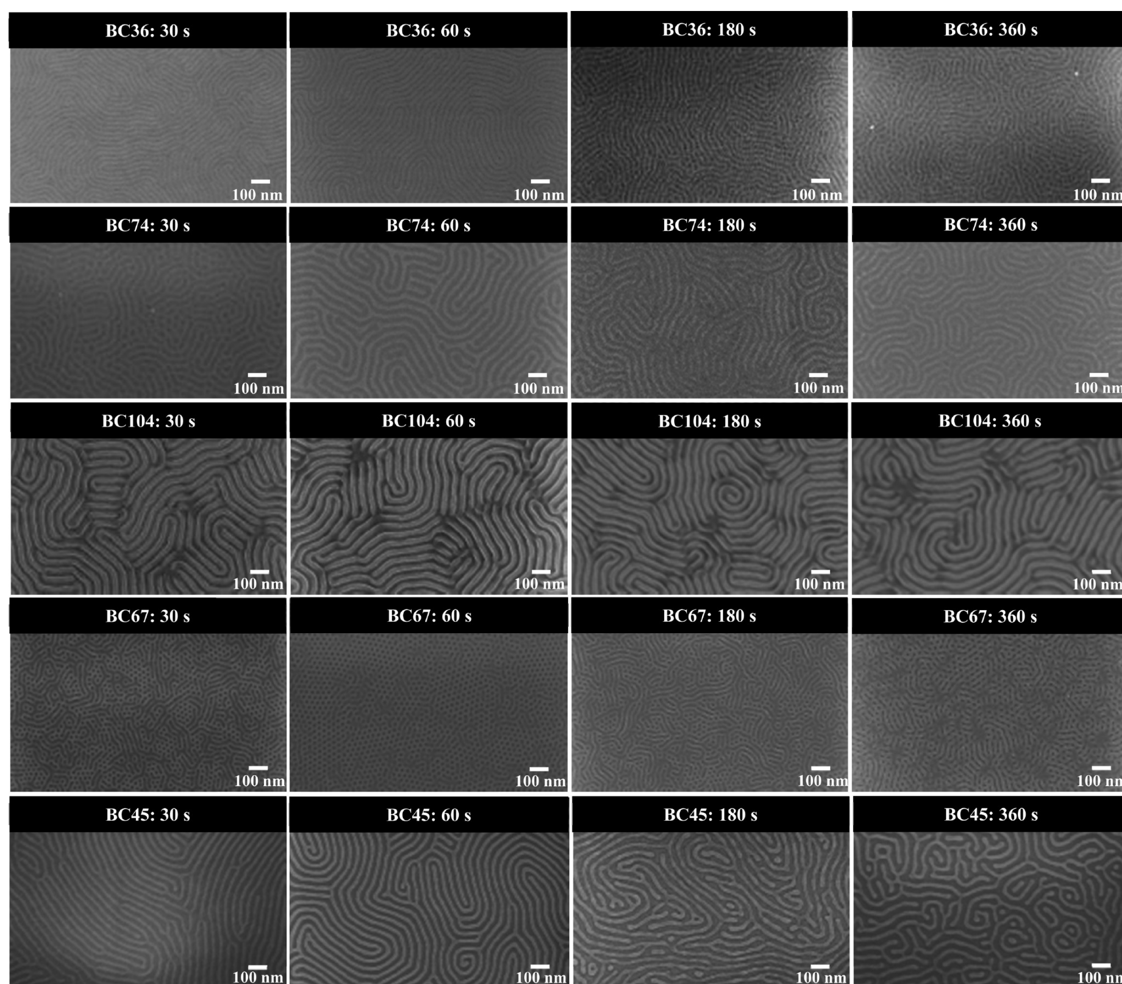

Figure 3. Top-down SEM images of the PS-*b*-PMMA and PS-*b*-PDMS BCPs films after selective plasma removal of the PMMA component, and the top PDMS wetting layer and partial PS matrix for PS-*b*-PMMA and PS-*b*-PDMS, respectively (light gray lines/matrix are PS/PDMS and darker lines/holes are voids created following PMMA/PS removal). The BCP films were microwave annealed at a target temperature of 323 K for different time periods as labeled in the images.

Si/SiO_2/bulk Si and Si_3N_4/bulk Si substrates had resistivities of ρ = 50–60, 10^{12}–10^{14}, 25–30, and 10^{14}–10^{16} Ω cm, respectively. The BCP films formed on these were microwave annealed at 323 K for 60 s for PS-*b*-PMMA and for 30 s for PS-*b*-PDMS BCPs. All films exhibited pattern formation. Figure 5 shows the results of the lamellar-forming PS-*b*-PMMA (BC36) on various substrates. Water contact angle measured on these surfaces after the brush grafting shows small variations in the hydrophobicity/hydrophilicity of the substrates as might be expected because of the use of the same polymer brush. The results presented in Figure 5 show a little correlation between the BCP ordering and the substrate resistivity. The results are inconsistent with the work of Buriak *et al.*,[43] which suggested that the oscillating electric field of the microwave irradiation excites positive carriers in doped silicon thereby converting microwave energy into thermal energy within the silicon substrate. However, our experiments are quite different in that temperature is strictly controlled and no solvent is used. In this way, the efficiency of substrate heating is less important because the microwave power is adjusted automatically. The results of PS-*b*-PDMS (BC45) on the same substrates are presented in Figure 5 and show similar behavior.

Microwave Assisted Directed Self-Assembly. The seminal work of Buriak *et al.*[43] demonstrated the compatibility of microwave anneal with graphoepitaxy for cylinder-forming PS-*b*-PMMA in the presence of solvent. The microwave assisted directed self-assembly demonstrated here for both lamellar- and cylinder-forming PS-*b*-PMMA in the absence of solvent. The patterned substrates with 250 and 500 nm pitches were grafted with HO-PS-*r*-PMMA brush prior to BCP deposition, and microwave annealed at 323 K for 60 s and related data are presented in Figure 6. It can be seen that the confinement topography induces excellent microphase segregation within the trenches irrespective of the channel width with lamella domains orientating perpendicular to the substrate surface, however, lacks long-range alignment in both BC36 and BC74. It is evident from Figure 6 that there is no preferential

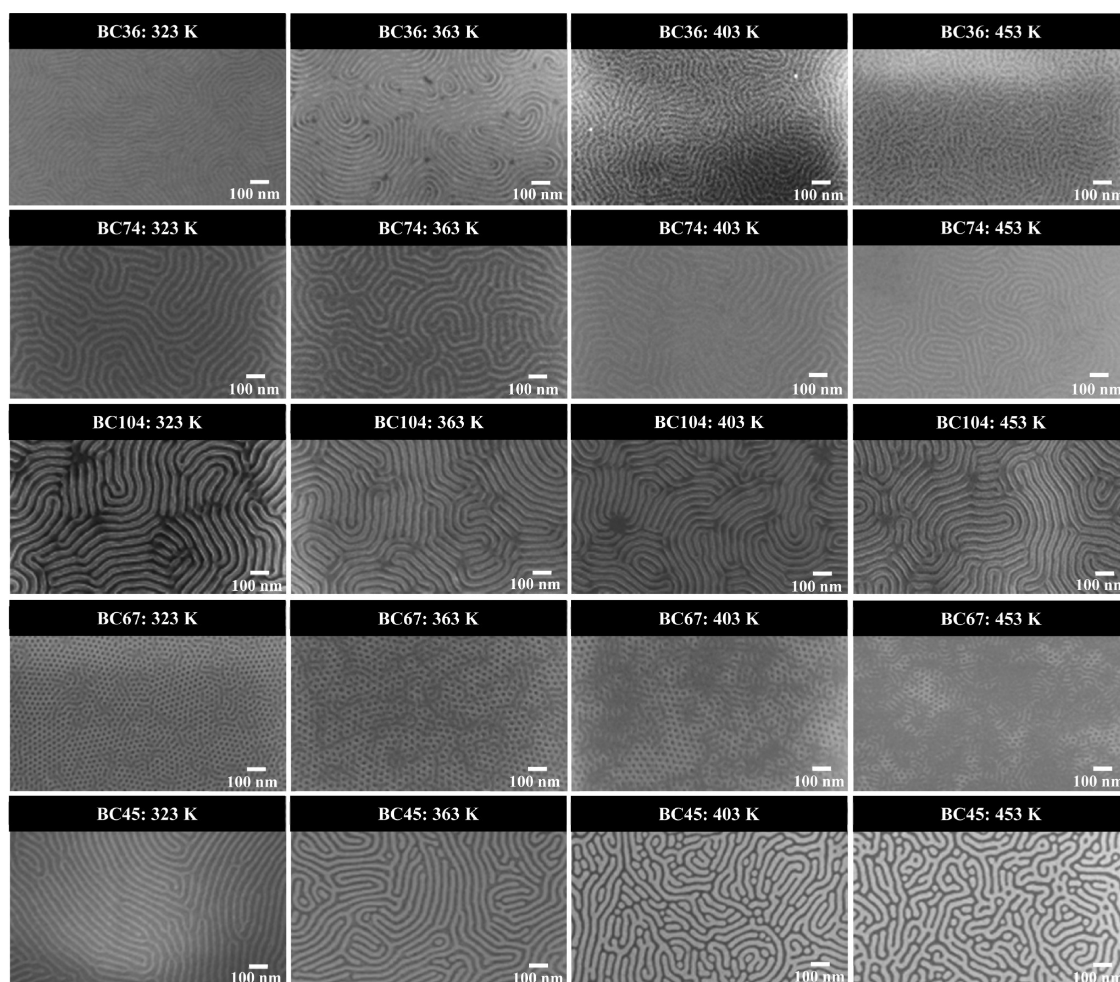

Figure 4. Top-down SEM images of the PS-*b*-PMMA and PS-*b*-PDMS BCPs films after selective plasma removal of the PMMA component, and the top PDMS wetting layer and partial PS matrix for PS-*b*-PMMA and PS-*b*-PDMS, respectively (light gray lines/matrix are PS/PDMS and darker lines/holes are voids created following PMMA/PS removal). The BCP films were microwave annealed at a target temperature as labeled in the images for 60 s for PS-*b*-PMMA and 30 s for PS-*b*-PDMS BCPs.

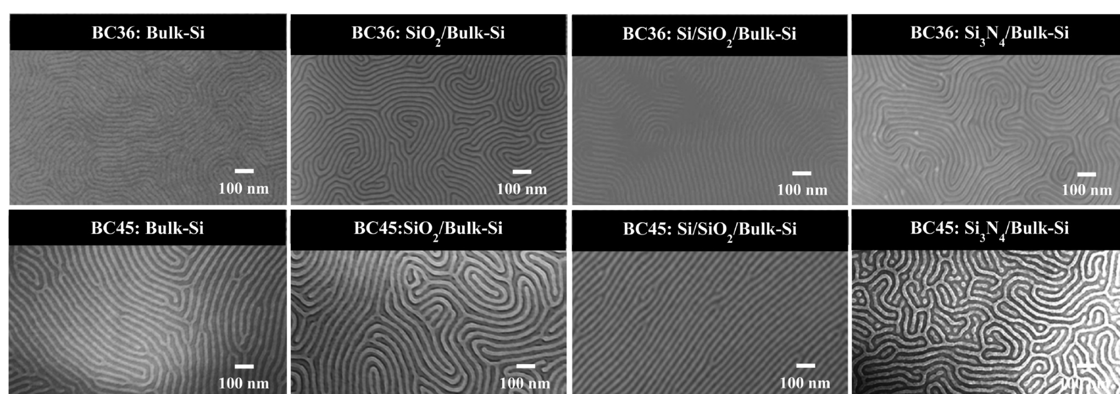

Figure 5. Top-down SEM images of PS-*b*-PMMA (BC36) and PS-*b*-PDMS (BC45) BCP films after selective plasma removal of the PMMA component, and the top PDMS wetting layer and partial PS matrix for PS-*b*-PMMA and PS-*b*-PDMS, respectively (light gray lines/matrix are PS/PDMS and darker lines/holes are voids created following PMMA/PS removal) on various substrates as labeled in the images. BCP films were microwave annealed at 323 K for 60 s for PS-*b*-PMMA and 30 s for PS-*b*-PDMS BCPs.

wetting of the sidewalls to either of the two blocks, PS and PMMA. The substrates were coated with HO-PS-*r*-PMMA before BCP deposition and the sidewalls being neutral wets the two blocks equally resulting in fingerprint type of patterns. The graphoepitaxy approach was also tried with the cylinder-forming BC67 under the same microwave anneal conditions. It can be seen from the results presented in Figure 6 that

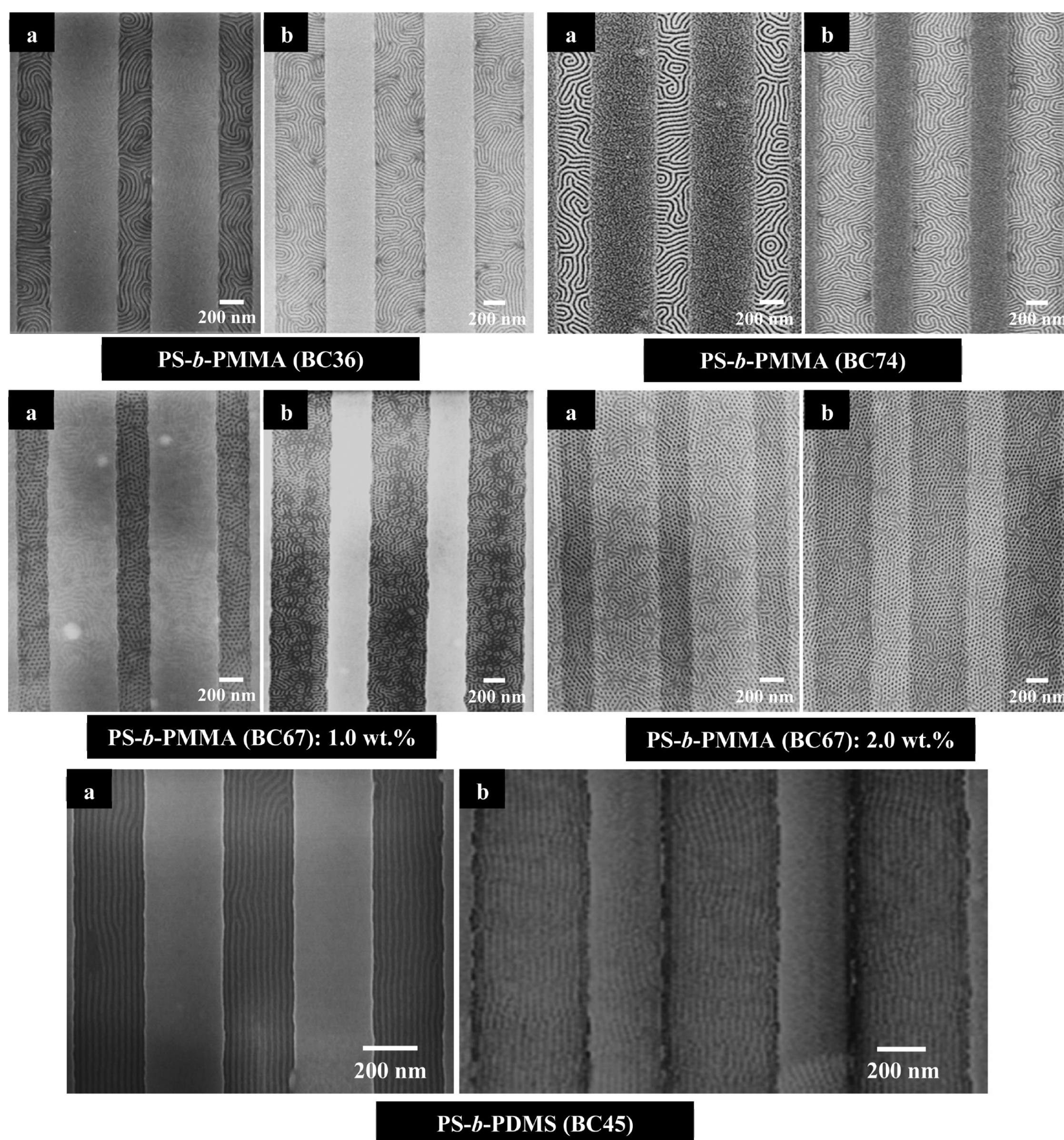

Figure 6. Top-down SEM images of PS-*b*-PMMA and PS-*b*-PDMS BCPs films after selective plasma removal of the PMMA component, and the top PDMS wetting layer and partial PS matrix for PS-*b*-PMMA and PS-*b*-PDMS, respectively (light gray lines/matrix are PS/PDMS and darker lines/holes are voids created following PMMA/PS removal) on patterned silicon substrates with channel pitches of (a) 250 nm and (b) 500 nm. BCP films were microwave annealed at 323 K for 60 s for PS-*b*-PMMA and 30 s for PS-*b*-PDMS BCPs.

perpendicular PMMA domain orientation was achieved within the trenches even with 1.0 wt % of the BCP solution unlike to planar substrate with good confinement. However, the polymer overflows the trenches with 2.0 wt % resulting in BCP patterns on the mesas.

The high χ factor enables PS-*b*-PDMS BCP to self-assemble with greater correlation length, and as such, the patterned substrates were precoated with PDMS−OH brush prior to BC45 deposition to direct self-assembly. Samples were microwave annealed at 323 K for 30 s based on the results demonstrated in Figures 3 **and** 4. The results of the PS-*b*-PDMS pattern after sequential CF_4 and O_2 etches is shown Figure 6. It can be seen from the images that the brush induced microphase segregation with graphoepitaxial alignment compatible with the pitches of the topographic patterns. Generally, for the hexagonal structure, preferred alignment should be achieved when the sidewalls preferentially interact with the majority block compared to the minor component. If the sidewalls are neutral and interact equally with both blocks (thus favoring the presence of both blocks at the sidewall), a disordered structure is formed. A good number of defects could be observed in the BCP patterns. However, this is not easy to quantify because a lot of defects observed arise from defects in the sidewall that cause local variations in the channel width. The results show that domain numbers can

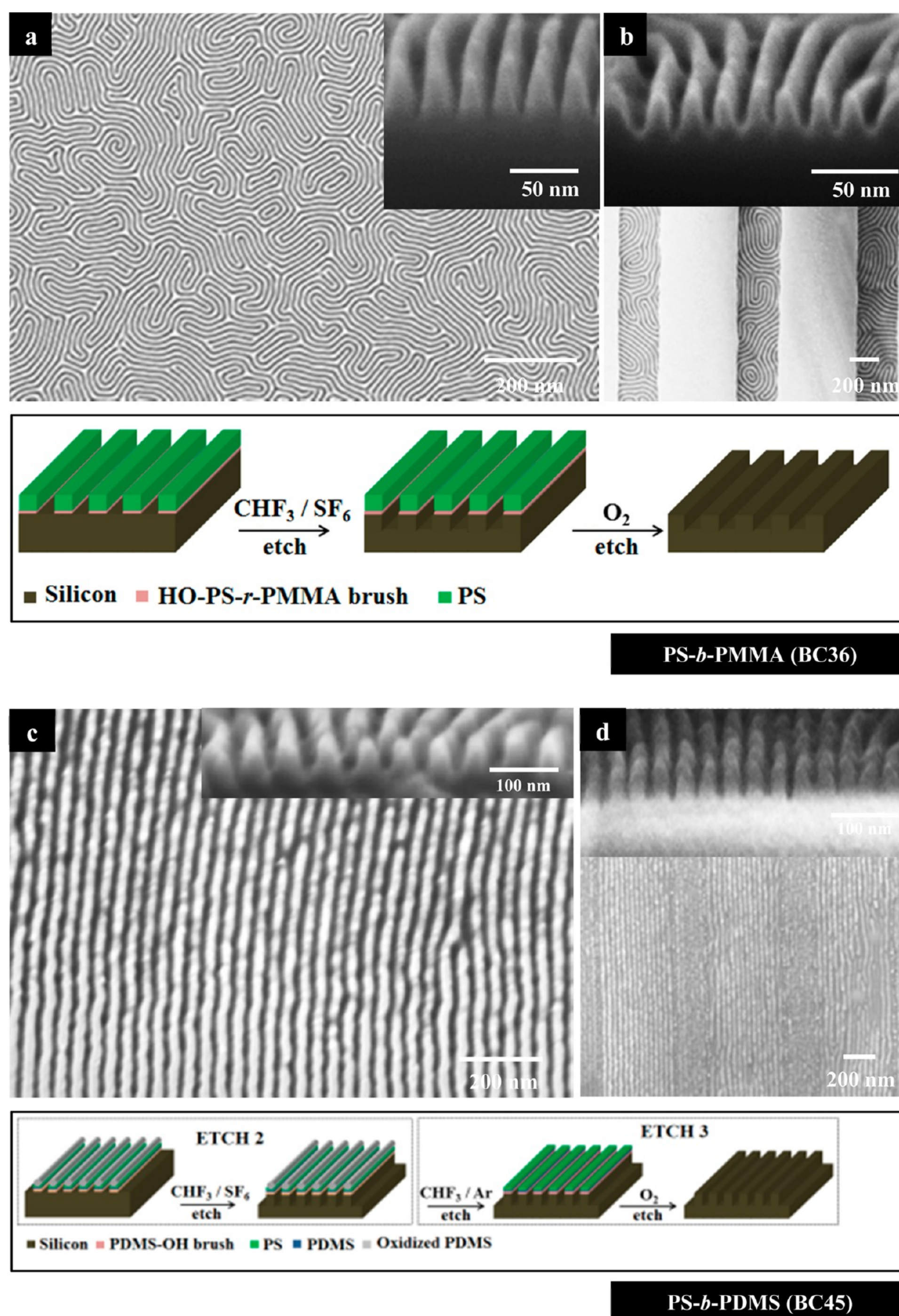

Figure 7. Top-down SEM images of PS soft mask template (fabricated from PS-*b*-PMMA (BC36)) patterns transferred to underlying (a) planar and (b) patterned silicon substrates (insets, (a and b) cross-sectional SEM images). SEM images of PDMS cylindrical patterns (fabricated from PS-*b*-PDMS (BC45)) transferred to underlying (c) planar and (d) patterned silicon substrates (insets, (c and d) cross-sectional SEM images). The schematics show the etching steps followed in the pattern transfer. See Experimental Section for details of pattern transfer in the two BCP systems.

be controlled by carefully tuning the pitch period of the patterns.

Pattern Transfer To Form Silicon Nanostructures. Attempts were made to pattern transfer the nanopatterns formed to the substrate surface. This is important not only to demonstrate the usefulness of the methodology for application in microelectronic fabrication, but also to show that the patterns observed are not simply surface features, but that the patterns observed are present through the depth of the film. Indicative results of successful pattern transfer are shown here for the PS-*b*-PMMA (BC36) and the PS-*b*-PDMS (BC45) systems.

The SEM images shown in Figure 7 of pattern transferred BC36 on both planar and patterned silicon substrates (note the microwave anneal is consistent with good filling of the channels as can be seen here)

are following a silicon etch for 9 s that generates the best quality features based on previous studies.[11−13] The silicon substrate now consists of topographically patterned lines corresponding to the parent PS mask. The cross-sectional image in the inset of Figure 7 provides a better view of the silicon features. The average silicon feature size and height measured from the SEM images is about 8.3 and 27 nm, respectively. This is because the etch process is not ideal in such narrow structures forming proportionally larger gaps between structures and more obviously nonrectangular feature cross sections (aspect ratio).

The complex morphology of PS-*b*-PDMS self-assembled patterns with a top and a bottom wetting PDMS layer makes pattern transfer to underlying silicon challenging as compared to the well-established polymer systems *e.g.*, PS-*b*-PMMA[11−13] and PS-*b*-PEO.[50] It should be noted that, for an effective pattern transfer process, the O_2 etch used in the initial etch has to be carefully optimized so that the cylinder structure is not undercut. However, if this is achieved, the oxidized, silica-like cylinders can act as hard mask for pattern transfer, an advantage with the BCP. The hard mask is unlikely to be affected by the etch recipe used to transfer the pattern into underlying silicon. Figure 7 shows the top-down and cross-sectional SEM images of the silicon nanowires on planar and patterned silicon substrates obtained after the etches were used to remove the silica-like materials at the substrate surface and then to selectively remove silicon. The cross-sectional SEM image shows the nanowire line width of ∼14.8 nm with a pattern depth of ∼42 nm. The cross-sectional SEM images shown in Figure 7 provide a more detailed image of the silicon nanowires fabricated in this way. Minor damage of the silicon features is apparent from Figure 7. The silicon features on the substrate are slightly narrower than the width of the initial oxidized PDMS cylinders due to partly isotropic etching. A reasonable aspect ratio of ∼1.25 was obtained. A comparison of pattern transfer of BC36 and BC45 reveals the superior fidelity of the silicon features with PDMS hard mask. The results demonstrated here shows the compatibility of microwave anneal process for nanofabrication and holds promise to commercialization.

DISCUSSIONS AND CONCLUSIONS

In this work, direct (*i.e.*, in the absence of a solvent) microwave assisted annealing has been shown to be effective in inducing controllable microphase separation in BCP thin films. The results are somewhat surprising since it is normally accepted that polymers are largely 'inert' to microwave radiation and will not increase significantly in temperature in conventional systems. Silicon substrates can be microwave heated, but this is not a facile process, and it is generally accepted that it is the intrinsic carriers not the dopant carriers that are responsible for heating.[51] Indeed, reports suggest that wafers with lower dopant levels heat more efficiently.[52] However, despite the range of substrates used, little dependence of the microphase separation was observed with substrate type, a result inconsistent with previous findings.[43]

In an effort to understand the data, the results of the nonconventional microwave annealing methodology reported in the present investigation are compared with complementary nonmicrowave, thermal annealing experiments under similar conditions of process temperature/time used in the microwave annealing experiments. The results are documented in the Supporting Information (Figures S3−S6) for clarity of presentation. The results from thermal annealing of the PS-*b*-PMMA BCPs under the low temperature/times used in a typical microwave process show little sign of regular microphase separation particularly with higher molecular weight systems. This is because the thermal experiments were performed well below the glass transition temperature of the PS-*b*-PMMA BCP. The PS-*b*-PDMS BCP system shows indications of microphase separation at higher anneal temperature and longer anneal time but with poor correlation length of the PDMS domains and with severe dewetting (Figures S4−S6) but compare very unfavorably to the data from microwave annealing of similar samples. These data suggest that microwave heating can bring about microphase separation at temperatures well below the glass transition temperature. However, indirect heating *via* the substrate might occur allowing the film temperature to be significantly greater than the instrument's set temperature. However, this seems less likely because of the range of substrates used. To confirm the passive role of the substrate, totally microwave inert substrates were investigated, and it was seen that microphase separation could be achieved at fused silica substrates in similar microwave process conditions (similar experiments were also carried out on glass and quartz). Indicative data are presented in Figure S7, and it is clear that the microphase separation behaviors of the two BCP systems are similar to the results obtained on bulk Si, SiO_2/bulk Si, Si/SiO_2/bulk Si and Si_3N_4/bulk Si substrates.

To understand the effect of substrate temperature during microwave anneal processes, temperature profiles from an independent sensor in the microwave chamber (Scheme S1) were recorded and representative examples are shown in Figure S8. The data presented in Figure S8 show that the actual temperature remains very close to the set temperature in an annealing experiment suggesting that local heating effects at the surface were not important. To confirm this suggestion, we further measured the actual temperature of the substrates in the (BCP + substrate) system using an infrared thermometer. The measured substrate temperatures were only 3−5 degrees lower (within experimental error) than the set temperature in the

microwave experiment. These data clearly demonstrate that the substrate is in equilibrium with the set temperature of the microwave experiment. Thus, it is evident that it is the microwave irradiation solely responsible for driving the self-organization in the BCP film.

This is a surprising result, but it can be noted that microwave heating is a commonly used method in the synthesis of organic compounds,[53−55] application in inorganic chemistry[56−59] and is also used polymer chemistry particularly in polymer curing.[60] Microwave irradiation is a dielectric heating process where molecular rotation occurs in materials containing polar molecules having an electrical dipole moment, with the consequence that they will align themselves in an electromagnetic field. In an oscillating field such as in an electromagnetic wave, these molecules rotate continuously aligning with it a process known as dipole rotation, or dipolar polarization where the molecules reverse direction as the field alternates. Under the influence of electrical forces, the rotating molecules impulse, twitch, and collide with other molecules, distributing the energy to adjacent molecules and atoms in the material and that energy appears as heat.[60−62] We suggest that, although polystyrene is microwave transparent, the other blocks in the BCPs *viz.*, polymethylmethacrylate and polydimethylsiloxane, are polar[63,64] and these polar molecules interact with the oscillating field resulting in dipole rotation and this rotation drives microphase separation. This may be through direct heating or *via* chain movements excited by the irradiating radiation.

In the setup used here, it appears from the time dependence of the pattern (which degrades on extended heating time) that the BCP film effectively moves from initial disorder to ordered microphase separation through to a more disordered structure at the longest anneal periods. These observations suggest that the polymer molecules are becoming progressively more 'excited' initially allowing chain movement to form the ordered phase and then becoming so mobile that any order is lost.

TABLE 2. Characteristics of Hydroxyl-Terminated Homopolymer (PDMS−OH), Random Copolymer (HO-PS-*r*-PMMA) Brushes, and Block Copolymers (PS-*b*-PMMA and PS-*b*-PDMS) Used for Present Study

M_n/ g mol^{-1}	polymer	designation	polydispersity index, M_w/M_n	PS mole fraction
12400	HO-PS-*r*-PMMA	RPB	1.25	0.58
5000	PDMS−OH	PDM	1.07	-
36000	PS-*b*-PMMA	BC36	1.07	0.46
74000	PS-*b*-PMMA	BC74	1.07	0.49
104000	PS-*b*-PMMA	BC104	1.09	0.49
67100	PS-*b*-PMMA	BC67	1.09	0.68
45500	PS-*b*-PDMS	BC45	1.15	0.60

In this way, the viability of the method for manufacture has been demonstrated. It has a number of advantages, notably in terms of process speed but it is also solventless and the use of large volume solvent annealing chambers is as yet unproven. The use of microwave annealing in silicon technology has been established on large wafer sizes.[52] Solvent annealing on large wafers offers problems because solvent condensation can induce large area defects, etc.[31] Further, the possibility of impurity incorporation is reduced by avoidance of the solvent. The use in semiconductor manufacture has been demonstrated by exploring the use of topographically patterned substrates and the ability of the technique to be used in pattern transfer to the substrate. In this way, the technique represents significant promise for future development.

EXPERIMENTAL SECTION

Materials. The BCPs and hydroxyl-terminated homopolymer and copolymer used in the present investigation were purchased from Polymer Source, Inc., Canada and detailed characteristics are summarized in Table 2. The substrates used were silicon ⟨100⟩ of p-type with a native oxide (SiO_2) layer of ∼2 nm thick (resistivity, ρ = 50−60 Ω cm), a silicon ⟨100⟩ substrate of p-type with 120 nm thick SiO_2 layer (resistivity, $\rho = 10^{12}-10^{14}$ Ω cm) and fused silica substrate. The oxide layers were deposited by a low-pressure chemical vapor deposition (LPCVD) method. We also used a p-doped silicon-on-insulator (SOI) (resistivity, ρ = 25−30 Ω cm) with a 20 nm device silicon layer separated through a 120 nm thick buried oxide (SiO_2) layer from the bulk silicon developed using separation by an oxygen implantation. The topographically patterned substrates used were p-type silicon ⟨100⟩ wafers with a LPCVD deposited silicon nitride (Si_3N_4) layer coated with a SiO_2 layer of ∼7 nm thick (resistivity, $\rho = 10^{14}-10^{16}$ Ω cm). These wafers were topographically patterned with channels of pitch 250 and 500 nm and depth of 50 nm (fabricated *via* 193 nm UV-lithography). It should be noted that all substrates gave similar results (since the surface chemistry is essentially due to silica) but were used to probe any substrate effects within the microwave process. Sulfuric acid, hydrogen peroxide, ethanol, acetone, isopropyl alcohol (IPA) and toluene were purchased from Sigma-Aldrich and used as received. Deionized (DI) water was used wherever necessary.

Substrate Precoating with Polymer Brushes and BCP Film Preparation. Substrates were diced into 0.5 cm^2 pieces and then degreased by ultrasonication in acetone and IPA solutions for 5 min each, dried in flowing N_2 gas, and baked for 2 min at 393 K in an ambient atmosphere to remove any residual IPA. This was followed by cleaning in a piranha solution (1:3 (v/v) 30% H_2O_2:H_2SO_4) (*CAUTION! May cause explosion in contact with organic material!*) at 363 K for 60 min; rinsed with DI water, acetone, and ethanol; and dried under N_2 flow. Hydroxyl-terminated polymer brush solutions of 1.0 wt % in toluene were spin-coated (P6700 Series Spin-coater, Specialty Coating Systems, Inc.) onto substrates at 3000 rpm for 30 s. Samples were annealed in a vacuum oven (Townson & Mercer EV018) at 443 K under vacuum (−100 kPa). This procedure provides chemically anchored brushes by condensation reactions between −OH groups at the substrate surface and on the brush. Unbound polymers were removed by ultrasonication (Cole-Palmer 8891 sonicator) and rinsing in toluene, and dried for 30 min at 333 K in an ambient atmosphere to remove any

residual toluene. A random HO-PS-*r*-PMMA brush has to be used to define orientation of the lamellae structure as perpendicular to the surface plane.[11−13] A PDMS brush orientates the PDMS cylinder structure parallel to the surface plane and allows good surface wetting.[31,41] BCPs (PS-*b*-PMMA and PS-*b*-PDMS) were dissolved in toluene to yield solutions of 0.7−3.0 wt % and then spin-coated onto the brush anchored surfaces at 3200 rpm for 30 s and immediately used for microwave irradiation.

Nonconventional Microwave Anneal of BCP Films. The microwave annealed experiments were performed in a microwave synthesizer, CEM Discover LabMate (CEM Microwave Technology Ltd., U.K.) with the IntelliVent Pressure Control System and CEM's Synergy software. The system has an *in-built* feature of focusing the microwaves with maximum efficiency into the sample cavity. CEM's Windows-based Synergy software was used to control the microwave parameters (power, temperature, time and pressure) as well as data handling. BCP-coated substrates were accommodated inside the reaction tube, which was sealed, placed inside the reaction chamber, and irradiated with microwave energy. The desired temperature was achieved through microwave feedback control, which required 20−100 s depending upon the target temperature. The preset anneal time started once the target temperature was achieved. It should be noted that sufficient microwave power was applied to achieve and hold the chosen temperature in reaction vessel. The anneal time considered was in the range of 30−360 s. It should be noted that the reaction vessel requires around 30−100 s to cool to ambient conditions following use. During this period, some organization and assembly is expected. The essential parameters, input power, temperature and pressure were recorded during the process. Dewetting of the BCP film was not observed in any of the experiments.

Conventional Thermal Anneal of BCP Films. BCP films were thermal annealed in the temperature range of 323−453 K under vacuum (−100 kPa) for 60−1800 s, to induce phase separation and evaporate any remaining solvent. Thin films were removed from the oven immediately after annealing and allowed to cool naturally in ambient.

Plasma Etching of BCP Films. The microwave annealed PS-*b*-PMMA films were subjected to selective removal of PMMA block by inductively coupled plasma (ICP) etches in an OIPT Plasmalab System 100 ICP180 etcher. The process was accomplished with an Ar/O_2 etch recipe of Ar (5 sccm) and O_2 (15 sccm) at 1.3 Pa and 100 W for 6 s to generate PS mask structures. Full details are given elsewhere.[11−13] It should be noted that, for process stability, the PS microdomains of the BCP film must interact the substrate sufficiently to retain the structural integrity of the film. It is accepted that the brush layer provides good film stability because the brush layer penetrates into the BCP thin films, thus anchoring it to the surface.[11−13,65,66] As can be seen below, it appears that the films retain this robustness *via* similar mechanism and suggests that the microwave anneal also allows interpenetration of brush layer and BCP domains.

PS-*b*-PDMS BCP films do not readily show the microphase separated structure because of the presence of a surface wetting layer of PDMS, which must be removed to reveal the domain structure.[31,41] Films were first treated with a CF_4 (15 sccm) plasma for 5 s with an ICP and reactive ion etching (RIE) powers of 400 and 30 W, respectively, at 2.0 Pa with a helium backside cooling pressure of 1333.2 Pa to remove any surface PDMS layer. This was followed by an O_2 (30 sccm) plasma for 10 s with an ICP and RIE powers of 1200 and 30 W, respectively, at 2.0 Pa with helium backside cooling pressure of 666.6 Pa. These steps follow similar methodology developed by Ross *et al.*[41] The process removes the PS component and forms an oxidized form of PDMS on the substrate. This etch step is referred as ETCH1.

Silicon Etch for Nanostructure Pattern Formation. For the PS-*b*-PMMA BCP, an SF_6/CHF_3 ICP etch was carried out on the samples using the PS structure as an etch masks. The etch used was carried out at 2.0 Pa and 500 W with SF_6 (15 sccm) and CHF_3 (80 sccm) for 9 s to transfer the template structure to underlying substrate. Remaining PS was removed using an O_2 (30 sccm) ash recipe at 2.0 Pa and 2000 W for 10 s.

The oxidized PDMS cylinders formed by the sequential CF_4 and O_2 etches were used as an etch mask for pattern transfer in PS-*b*-PDMS BCP by an etch process designated as ETCH2. The pattern transfer step involved an initial CHF_3 (80 sccm) and Ar (30 sccm) plasma etch for 5 s with an ICP and RIE powers of 400 and 30 W, respectively, at 1.6 Pa to remove any residual PDMS wetting layer at the substrate surface. This milder etch treatment was critical and needed careful optimization. It was used to remove passive silica and any PDMS components at the silicon substrate surface without removing the 'etch mask' formed by the oxidized PDMS cylinders. This process was followed by a selective silicon etch using CHF_3 (80 sccm) and SF_6 (15 sccm) gases for 15 s with an ICP and RIE powers of 1200 and 30 W, respectively, at 2.0 Pa with helium backside cooling pressure of 1333.2 Pa to transfer the patterns into the underlying substrate. The polymers remained after pattern transfer was removed by ETCH3. The residual oxidized PDMS cylinders were removed by a 10 s silica (SiO_2) etch based on CHF_3 (80 sccm) and Ar (15 sccm) gases with an ICP and RIE powers of 1200 and 40 W, respectively, at 2.0 Pa with a helium backside cooling pressure of 1333.2 Pa. This is followed by 5 s O_2 (30 sccm) etch to remove the residual PS matrix and polymer brush underneath with an ICP and RIE powers of 2000 and 100 W, respectively, at 1.3 Pa with a helium backside cooling pressure of 666.6 Pa. The etching processes were accomplished in an OIPT Plasmalab System100 ICP180 etch tool.

Characterization of Materials. Advancing contact angles (θ_a) of deionized water on the substrates were measured using a Data Physics Contact Angle (model: OCA15) goniometer. Contact angles were measured on the opposite edges of at least five drops and averaged. The values were reproducible to within 1.5°.

BCP film thicknesses were measured with a spectroscopic ellipsometer "Plasmos SD2000 Ellipsometer" at a fixed angle of incidence of 70°, on at least five different places on the sample. A two-layer model (SiO_2 + polymer brush) for polymer brushes and a three-layer model (SiO_2 + polymer brush + BCP) for total BCP films were used to simulate experimental data.

The actual temperatures of the substrates in the (BCP + substrate) systems were measured by an Infrared Thermometer (SMART SENSOR, AR330 (−32 to 330 °C)) immediately after the microwave experiment.

An IR 610, Varian infrared spectrometer was used to record the FTIR spectra. The measurements were performed in the spectral range of 4000−500 cm^{-1}, with a resolution of 4 cm^{-1} and data averaged over 32 scans.

An Atomic Force Microscope (DME 2452 DualScope Scanner DS AFM) was operated in AC (tapping) mode under ambient conditions using silicon microcantilever probe tips with a force constant of 60 000 N m^{-1} and a scanning force of 0.11 nN. Topographic and phase images were recorded simultaneously. Fast Fourier Transforms (FFT) of the topographic images was used to measure the degree of alignment and the presence of defects/nonregular patterns.

SEM images were obtained by a high resolution (<1 nm) Field Emission Zeiss Ultra Plus-SEM with a Gemini column operating at an accelerating voltage of 5 kV.

Conflict of Interest: The authors declare no competing financial interest.

Supporting Information Available: TEM cross-sectional image of HO-PS-*r*-PMMA brush coated silicon substrate, AFM topography images of microwave annealed PS-*b*-PMMA BCP films of various molecular weights, and AFM topography, SEM images of nonmicrowave annealed BCP films, schematic of temperature sensor and representative temperature profiles. This material is available free of charge *via* the Internet at http://pubs.acs.org.

Acknowledgment. Financial support for this work is provided by the EU FP7 NMP project, LAMAND (grant number 245565) project and the Science Foundation Ireland (grant number 09/IN.1/602), and gratefully acknowledged.

REFERENCES AND NOTES

1. *International Technology Roadmap for Semiconductors*, 2007 ed.; Emerging Research Materials; Semiconductor Industry Association: San Jose, CA, 2007.
2. Harriott, L. Limits of Lithography. *Proc. IEEE* **2001**, *89*, 366–374.
3. Ito, T.; Okazaki, S. Pushing the Limits of Lithography. *Nature* **2000**, *406*, 1027–1031.
4. Broers, A. N. Resolution Limits for Electron-Beam Lithography. *IBM J. Res. Dev.* **1988**, *32*, 502–513.
5. Black, C. T. Polymer Self-Assembly as a Novel Extension to Optical Lithography. *ACS Nano* **2007**, *1*, 147–150.
6. Thurn-Albrecht, T.; Schotter, J.; Kastle, G. A.; Emley, N.; Shibauchi, T.; Krusin Elbaum, L.; Guarini, K.; Black, C. T.; Tuominen, M. T.; Russell, T. P. Ultrahigh-Density Nanowire Arrays Grown in Self-assembled Diblock Copolymer Templates. *Science* **2000**, *290*, 2126–2129.
7. Thurn-Albrecht, T.; Steiner, R.; DeRouchey, J.; Stafford, C. M.; Huang, E.; Bal, M.; Tuominen, M.; Hawker, C. J.; Russell, T. P. Nanoscopic Templates from Oriented Block Copolymer Films. *Adv. Mater.* **2000**, *12*, 787–791.
8. Yang, S. Y.; Ryu, I.; Kim, H. Y.; Kim, J. K.; Jang, S. K.; Russell, T. P. Nanoporous Membranes with Ultrahigh Selectivity and Flux for the Filtration of Viruses. *Adv. Mater.* **2006**, *18*, 709–712.
9. Holden, G.; Legge, N. R.; Schroeder, H. E.; Quirk, R. P. *Thermoplastic Elastomers*; Hanser: New York, 1987.
10. Hamley, I. W. *The Physics of Block Copolymers*; Oxford University Press: New York, 1998.
11. Rasappa, S.; Borah, D.; Senthamaraikannan, R.; Faulkner, C. M.; Shaw, M. T.; Gleeson, P.; Holmes, J. D.; Morris, M. A. Block Copolymer Lithography: Feature Size Control and Extension by an Over-Etch Technique. *Thin Solid Films* **2012**, *522*, 318–323.
12. Farrell, R. A.; Kinahan, N. T.; Hansel, S.; Stuen, K. O.; Petkov, N.; Shaw, M. T.; West, L. E.; Djara, V.; Dunne, R. J.; Varona, O. G.; *et al.* Large-Scale Parallel Arrays of Silicon Nanowires *via* Block Copolymer Directed Self-Assembly. *Nanoscale* **2012**, *4*, 3228–3236.
13. Borah, D.; Shaw, M. T.; Rasappa, S.; Farrell, R. A.; O'Mahony, C.; Faulkner, C. M.; Bosea, M.; Gleeson, P.; Holmes, J. D.; Morris, M. A. Plasma Etch Technologies for the Development of Ultra-Small Feature Size Transistor Devices. *J. Phys. D: Appl. Phys.* **2011**, *44*, 174012–174023.
14. Park, S. M.; Liang, X.; Harteneck, B. D.; Pick, T. E.; Hiroshiba, N.; Wu, Y.; Helms, B. A.; Olynick, D. L. Sub-10 nm Nanofabrication *via* Nanoimprint Directed Self-assembly of Block Copolymers. *ACS Nano* **2011**, *5*, 8523–8531.
15. Jeong, S. J.; Kim, J. E.; Moon, H. S.; Kim, B. H.; Kim, S. M.; Kim, J. B.; Kim, S. O. Soft Graphoepitaxy of Block Copolymer Assembly with Disposable Photoresist Confinement. *Nano Lett.* **2009**, *9*, 2300–2305.
16. Farrell, R. A.; Fitzgerald, T. G.; Borah, D.; Holmes, J. D.; Morris, M. A. Chemical Interactions and Their Role in the Microphase Separation of Block Copolymer Thin Films. *Int. J. Mol. Sci.* **2009**, *10*, 3671–3712.
17. Bang, J.; Jeong, U.; Ryu, D. Y.; Russell, T. P.; Hawker, C. J. Block Copolymer Nanolithography: Translation of Molecular Level Control to Nanoscale Patterns. *Adv. Mater.* **2009**, *21*, 4769–4792.
18. Chai, J.; Wang, D.; Fan, X.; Buriak, J. M. Assembly of Aligned Linear Metallic Patterns on Silicon. *Nat. Nanotechnol.* **2007**, *2*, 500–506.
19. Park, S. M.; Stoykovich, M. P.; Ruiz, R.; Zhang, Y.; Black, C. T.; Nealey, P. F. Directed Assembly of Lamellae- Forming Block Copolymers by Using Chemically and Topographically Patterned Substrates. *Adv. Mater.* **2007**, *19*, 607–611.
20. Ruiz, R.; Ruiz, N.; Zhang, Y.; Sandstrom, R. L.; Black, C. T. Local Defectivity Control of 2D Self-Assembled Block Copolymer Patterns. *Adv. Mater.* **2007**, *19*, 2157–2162.
21. Xiao, S.; Yang, X. M.; Edwards, E. W.; La, Y.-H.; Nealey, P. F. Graphoepitaxy of Cylinder-Forming Block Copolymers for Use as Templates to Pattern Magnetic Metal Dot Arrays. *Nanotechnology* **2005**, *16*, S324–S329.
22. Segalman, R. A.; Yokoyama, H.; Kramer, E. J. Graphoepitaxy of Spherical Domain Block Copolymer Films. *Adv. Mater.* **2001**, *13*, 1152–1155.
23. Han, E.; Kang, H.; Liu, C.-C.; Nealey, P. F.; Gopalan, P. Graphoepitaxial Assembly of Symmetric Block Copolymers on Weakly Preferential Substrates. *Adv. Mater.* **2010**, *22*, 4325–4329.
24. Ji, S.; Liu, C.-C.; Son, J. G.; Gotrik, K.; Gordon, S. W. C.; Gopalan, P.; Himpsel, F. J.; Char, K.; Nealey, P. F. Generalization of the Use of Random Copolymers to Control the Wetting Behavior of Block Copolymer Films. *Macromolecules* **2008**, *41*, 9098–9103.
25. Han, E.; In, I.; Park, S. M.; La, Y. H.; Wang, Y.; Nealey, P. F.; Gopalan, P. Photopatternable Imaging Layers for Controlling Block Copolymer Microdomain Orientation. *Adv. Mater.* **2007**, *19*, 4448–4452.
26. Ryu, D. Y.; Wang, J. Y.; Lavery, K. A.; Drockenmuller, E.; Satija, S. K.; Hawker, C. J.; Russell, T. P. Surface Modification with Cross-Linked Random Copolymers: Minimum Effective Thickness. *Macromolecules* **2007**, *40*, 4296–4300.
27. In, I.; La, Y. H.; Park, S. M.; Nealey, P. F.; Gopalan, P. Side-Chain Grafted Random Copolymer Brushes as Neutral Surfaces for Controlling the Orientation of Block Copolymer Microdomains in Thin Films. *Langmuir* **2006**, *22*, 7855–7860.
28. Ryu, D. Y.; Shin, K.; Drockenmuller, E.; Hawker, C. J.; Russell, T. P. A Generalized Approach to the Modification of Solid Surfaces. *Science* **2005**, *308*, 236–239.
29. Ludwigs, S.; Schmidt, K.; Stafford, C. M.; Amis, E. J.; Fasolka, M. J.; Karim, A.; Magerle, R.; Krausch, G. Combinatorial Mapping of the Phase Behavior of ABC Triblock Terpolymers in Thin Films: Experiments. *Macromolecules* **2005**, *38*, 1850–1858.
30. Huang, E.; Russell, T. P.; Harrison, C.; Chaikin, P. M.; Register, R. A.; Hawker, C. J.; Mays, J. Using Surface Active Random Copolymers to Control the Domain Orientation in Diblock Copolymer Thin Films. *Macromolecules* **1998**, *31*, 7641–7650.
31. Hobbs, R. G.; Farrell, R. A.; Bolger, C. T.; Kelly, R. A.; Morris, M. A.; Petkov, N.; Holmes, J. D. Selective Sidewall Wetting of Polymer Blocks in Hydrogen Silsesquioxane Directed Self-Assembly of PS-*b*-PDMS. *ACS Appl. Mater. Interfaces* **2012**, *4*, 4637–4642.
32. Chang, J.-B.; Son, J. G.; Hannon, A. F.; Alexander-Katz, A.; Ross, C. A.; Berggren, K. K. Aligned Sub-10-nm Block Copolymer Patterns Templated by Post Arrays. *ACS Nano* **2012**, *6*, 2071–2077.
33. Son, J. G.; Chang, J.-B.; Berggren, K. K.; Ross, C. A. Assembly of Sub-10-nm Block Copolymer Patterns with Mixed Morphology and Period Using Electron Irradiation and Solvent Annealing. *Nano Lett.* **2011**, *11*, 5079–5084.
34. Voet, V. S. D.; Pick, T. E.; Park, S.-M.; Moritz, M.; Hammack, A. T.; Urban, J. J.; Ogletree, D. F.; Olynick, D. L.; Helms, B. A. Interface Segregating Fluoralkyl-Modified Polymers for High-Fidelity Block Copolymer Nanoimprint Lithography. *J. Am. Chem. Soc.* **2011**, *133*, 2812–2815.
35. Jung, Y. S.; Chang, J. B.; Verploegen, E.; Berggren, K. K.; Ross, C. A. A Path to Ultranarrow Patterns Using Self-Assembled Lithography. *Nano Lett.* **2010**, *10*, 1000–1005.
36. Jung, Y. S.; Lee, J. H.; Lee, J. Y.; Ross, C. A. Fabrication of Diverse Metallic Nanowire Arrays Based on Block Copolymer Self-Assembly. *Nano Lett.* **2010**, *10*, 3722–3726.
37. Jung, Y. S.; Ross, C. A. Solvent-Vapor-Induced Tunability of Self-Assembled Block Copolymer Patterns. *Adv. Mater.* **2009**, *21*, 2540–2545.
38. Bita, I.; Wang, J. K. W.; Jung, Y. S.; Ross, C. A.; Thomas, E. L.; Berggren, K. K. Graphoepitaxy of Self-Assembled Block Copolymers on Two-Dimensional Periodic Patterned Templates. *Science* **2008**, *321*, 939–943.
39. Jung, Y. S.; Jung, W.; Ross, C. A. Nanofabricated Concentric Ring Structures by Templated Self-Assembly of a Diblock Copolymer. *Nano Lett.* **2008**, *8*, 2975–2981.
40. Ross, C. A.; Jung, Y. S.; Chuang, V. P.; Llievski, F.; Yang, J. K. W.; Bita, I.; Thomas, E. L.; Smith, H. I.; Berggren, K. K.; Vancso, G. J.; *et al.* Si-Containing Block Copolymers for Self-Assembled Nanolithography. *J. Vac. Sci. Technol., B* **2008**, *26*, 2489–2494.
41. Jung, Y. S.; Ross, C. A. Orientation-Controlled Self-Assembled Nanolithography Using a Polystyrene-Polydimethylsiloxane Block Copolymer. *Nano Lett.* **2007**, *7*, 2046–2050.

42. Zhang, X.; Murphy, J. N.; Wu, N. L. Y.; Harris, K. D.; Buriak, J. M. Rapid Assembly of Nanolines with Precisely Controlled Spacing from Binary Blends of Block Copolymers. *Macromolecules* **2011**, *44*, 9752–9757.
43. Zhang, X.; Harris, K. D.; Wu, N. L. Y.; Murphy, J. N.; Buriak, J. M. Fast Assembly of Ordered Block Copolymer Nanostructures Through Microwave Annealing. *ACS Nano* **2010**, *4*, 7021–7029.
44. Jeong, U.; Ryu, D. Y.; Kim, K. J.; Kim, D. H.; Russell, T. P.; Hawker, C. J. Volume Contractions Induced by Crosslinking: A Novel Route to Nanoporous Polymer Films. *Adv. Mater.* **2003**, *15*, 1247–1250.
45. Kirk, C. T. Quantitative Analysis of the Effect of Disorder-Induced Mode Coupling on Infrared Absorption in Silica. *Physical Review B.* **1998**, *38*, 1255–1273.
46. Zhang, X.; Douglas, J. F.; Jones, R. L. Influence of Film Casting Method on Block Copolymer Ordering in Thin Films. *Soft Matter* **2012**, *8*, 4980–4987.
47. Ryu, D. Y.; Ham, S.; Kim, E.; Jeong, U.; Hawker, C. J.; Russell, T. P. Cylindrical Microdomain Orientation of PS-*b*-PMMA on the Balanced Interfacial Interactions: Composition Effect of Block Copolymers. *Macromolecules* **2009**, *42*, 4902–4906.
48. Zhang, X.; Berry, B. C.; Yager, K. G.; Kim, S.; Jones, R. L.; Satija, S.; Pickel, D. L.; Douglas, J. F.; Karim, A. Surface Morphology Diagram for Cylinder-Forming Block Copolymer Thin Films. *ACS Nano* **2008**, *2*, 2331–2341.
49. Xuan, Y.; Peng, J.; Cui, L.; Wang, H.; Li, B.; Han, Y. Morphology Development of Ultrathin Symmetric Diblock Copolymer Film *via* Solvent Vapor Treatment. *Macromolecules* **2004**, *37*, 7301–7307.
50. Ghoshal, T.; Maity, T.; Godsell, J. F.; Roy, S.; Morris, M. A. Large Scale Monodisperse Hexagonal Arrays of Super Paramagnetic Iron Oxides Nanodots: A Facile Block Copolymer Inclusion Method. *Adv. Mater.* **2012**, *24*, 2390–2397.
51. Kwong, D.-L. *Rapid Thermal and Other Short-Time Processing Technologies II: Proceedings of the International Symposium*; The Electrochemical Society: Pennington, NJ, 2001.
52. Zohm, H.; Kasper, E.; Mehringer, P.; Muller, G. A. Thermal Processing of Silicon Wafers with Microwave Co-Heating. *Microelectron. Eng.* **2000**, *54*, 247–253.
53. Larhed, M.; Olofsson, K. *Microwave Methods in Organic Synthesis*; Springer: Berlin, Germany, 2006.
54. Kappe, C. O.; Stadler, A. *Microwaves in Organic and Medicinal Chemistry*; Wiley-VCH: Weinheim, Germany, 2005.
55. Lidstrom, P.; Tierney, J. P., Eds. *Microwave-Assisted Organic Synthesis*; Blackwell Publishing: Oxford, U.K., 2005.
56. Chou, Y.-H.; Morgan, A. J.; Hondow, N. S.; Brydson, R.; Douthwaite, R. E. Microwave-Induced Plasma Heating and Synthesis: *In Situ* Temperature Measurement of Metal Oxides and Reactions to form Ternary Oxides. *Dalton Trans.* **2010**, *39*, 6062–6066.
57. Douthwaite, R. E. Microwave-Induced Plasma-Promoted Materials Synthesis. *Dalton Trans.* **2007**, 1002–1005.
58. Whittaker, A. G. Diffusion in Microwave-Heated Ceramics. *Chem. Mater.* **2005**, *17*, 3426–3432.
59. Rao, K. J.; Vaidhyanathan, B.; Ganguli, M.; Ramakrishnan, P. A. Synthesis of Inorganic Solids Using Microwaves. *Chem. Mater.* **1999**, *11*, 882–895.
60. Galema, S. A. Microwave Chemistry. *Chem. Soc. Rev.* **1997**, *26*, 233–238.
61. Gabriel, C.; Gabriel, S.; Grant, E. H.; Halstead, B. S. J.; Mingos, D. M. P. Dielectric Parameters Relevant to Microwave Dielectric Heating. *Chem. Soc. Rev.* **1998**, *27*, 213–223.
62. Mingos, D. M. P.; Baghurst, D. R. Applications of Microwave Dielectric Heating Effects to Synthetic Problems in Chemistry. *Chem. Soc. Rev.* **1991**, *20*, 1–47.
63. Ando, H.; Yoshizaki, T.; Aoki, A.; Yamakawa, H. Mean-Square Electric Dipole Moment of Oligo- and Poly(methylmethacrylate)s in Dilute Solution. *Macromolecules* **1997**, *30*, 6199–6207.
64. Konishi, T.; Yoshizaki, T.; Yamakawa, H. On the "Universal Constants" ρ and ϕ of Flexible Polymers. *Macromolecules* **1991**, *24*, 5614–5622.
65. Mansky, P.; Liu, Y.; Huang, E.; Russell, T. P.; Hawker, C. Controlling Polymer-Surface Interactions with Random Copolymer Brushes. *Science* **1997**, *275*, 1458–1460.
66. Mansky, P.; Russell, T. P.; Hawker, C. J.; Mays, J.; Cook, D. C.; Satija, S. K. Interfacial Segregation in Disordered Block Copolymers: Effect of Tunable Surface Potentials. *Phys. Rev. Lett.* **1997**, *79*, 237–240.